Hierarchical Bandwidth Modulations for Ultra-Broadband Communications in the Terahertz Band

Duschia Bodet[©], Student Member, IEEE, Priyangshu Sen, Student Member, IEEE,

Zahed Hossain, Member, IEEE, Ngwe Thawdar, Member, IEEE, and Josep M. Jornet¹⁰, Senior Member, IEEE

Abstract—Terahertz (THz)-band (0.1-10 THz) communication will be key in enabling high speed wireless links due to the wide available bandwidths. At THz frequencies, the path-loss is governed by high spreading loss due to small antenna apertures and by molecular absorption loss due to water vapor. The latter also determines the available transmission bandwidth, which shrinks with distance. Modulations that consider the high propagation loss and the distance-dependent bandwidth are needed to fully exploit the THz channel's bandwidth. Using a hierarchical constellation to simultaneously service users at symbol rates, Hierarchical Bandwidth Modulation (HBM) leverages molecular absorption to increase aggregate data rates in a broadcast system while offering flexibility to receivers experiencing high path loss. This paper introduces HBM and evaluates its performance. The symbol error rate performance for a 4/M-QAM HBM system is derived and verified using simulations. These results are used to define the design constraints for an HBM system: the HBM functional region and transition region. The functional region is verified using an experimental testbed for ultrabroadband communications. The results show that with proper design HBM successfully achieves its goal to exploit the distance-dependent characteristics of the THz channel, to spatially multiplex users, and to increase the system capacity.

Index Terms—Terahertz communications, ultrabroadband networks, 6G, hierarchical modulations, absorption loss.

I. INTRODUCTION

THE growing demand for ubiquitous communication in today's world has caused the wireless spectrum below 10 GHz to become increasingly congested. As a result, more

Manuscript received 24 January 2022; revised 8 July 2022; accepted 4 September 2022. Date of publication 27 September 2022; date of current version 10 March 2023. This work was supported in part by the U.S. National Science Foundation (NSF) under Grant CNS-1730148 and Grant CNS-2011411 and in part by the United States Air Force Research Laboratory under Grant FA8750-20-1-0200. Approved for public release. Case # AFRL-2022-0907. An earlier version of this paper was presented at IEEE International Conference on Communications [DOI: 10.1109/ICC.2019.8761547]. The associate editor coordinating the review of this article and approving it for publication was J. Hamalainen. (Corresponding author: Duschia Bodet.)

Duschia Bodet, Priyangshu Sen, and Josep M. Jornet are with the Department of Electrical and Computer Engineering, Northeastern University, Boston, MA 02115 USA (e-mail: bodet.d@northeastern.edu; sen.pr@northeastern.edu; jmjornet@northeastern.edu).

Zahed Hossain was with the Department of Electrical Engineering, University at Buffalo, The State University of New York, Buffalo, NY 14260 USA. He is now with Intel Corporation, Hillsboro, OR 97124 USA (e-mail: zahed.hossain@intel.com).

Ngwe Thawdar is with the Air Force Research Laboratory, Rome, NY 13441 USA (e-mail: ngwe.thawdar@us.af.mil).

Color versions of one or more figures in this article are available at https://doi.org/10.1109/TWC.2022.3207966.

Digital Object Identifier 10.1109/TWC.2022.3207966

spectrum is needed to supply the desired connectivity, and the Terahertz (THz) band, from 0.1 to 10 THz, is a prime candidate for providing this required spectrum. Although they have primarily been limited to sensing applications [1], THz signals have significant potential for wireless communications due to their large available bandwidths. These bandwidths - on the order of tens of GHz [2] - are predicted to be key to wirelessly connecting the 13.1 billion mobile devices that are projected to be in use by 2023 [3]. In addition to providing the necessary spectrum to support more devices, the bandwidth available in the THz band could also be used to provide faster single user or aggregate data rates. Given the rapid growth of the Internet of Things (IoT), the demand for wireless Terabit-per-second (Tbps) links is expected to become realized within one to five years [3], and the THz band has the ability to provide the necessary spectrum for such links [4], [5], [6].

Although THz communications present exciting opportunities, they have their own set of challenges that must be addressed before they can reach their full potential. Chief among these challenges are the high path losses and distancedependent bandwidth experienced by THz signals due to the small wavelength and molecular absorption. In this work, we present Hierarchical Bandwidth Modulation (HBM) to address these challenges. HBM is an extension of traditional hierarchical modulation (HM) that introduces a hierarchy in bandwidth by simultaneously servicing users at different symbol rates. The concept of changing the symbol rate in multi-resolution constellations is a novel approach motivated by the distance-dependent bandwidth in the THz band. First proposed in [7], HBM uses the THz band's molecular absorption losses to increase the data rate of single-transmitter multiple-receiver (STMR) systems and to multiplex users in space. To our knowledge, it is the only work that leverages the THz channel's high path loss to increase the system's overall data rate and offer a solution for high propagation loss scenarios across a range of frequencies.

In this paper, we expand on the work presented in [7] to propose, fully characterize, and experimentally verify HBM as a novel approach in waveform design that capitalizes on the high path losses in the THz band.

The contributions of this paper are as follows:

 We present HBM as a novel modulation scheme to exploit the THz channel's high path losses in a way

1536-1276 © 2022 IEEE. Personal use is permitted, but republication/redistribution requires IEEE permission. See https://www.ieee.org/publications/rights/index.html for more information.

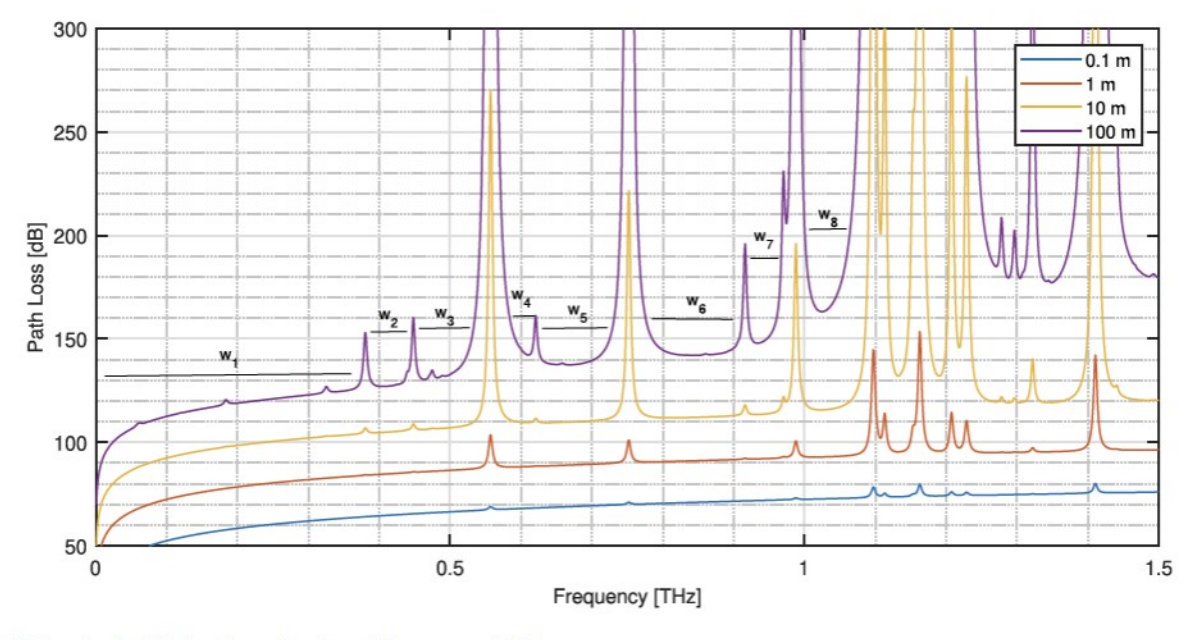


Fig. 1. Path Loss in the THz band as a function of frequency and distance.

that multiplexes users in space and increases the overall system data rate.

- We derive the error rate performance for 4/M-QAM HBM receivers.
- We define the HBM functional region necessary for designing a successful HBM systems.
- We suggest a transition region for receivers experiencing fluctuating channels.
- We verify our error rate derivations with full end-to-end simulations of a THz transmitter, channel, and receiver in MATLAB.
- We experimentally verify the existence of the HBM functional region in the THz band.

The remainder of this paper is organized as follows. In Sec. II we describe the relevant related works. This is followed by Sec. III, where we describe HBM in detail and propose a modulator structure. Next, in Sec. IV, we derive the symbol error rate (SER) for HBM receivers in the 4/16-QAM and 4/M-QAM cases. We further discuss these derived expressions and compare HBM's acheivable data rates to that of traditional HM in Sec. V. Then, in Sec. VI, we present the HBM functional region and transition region. We proceed to verify our derived SER expressions through simulation and to experimentally verify the existence of the functional region in Sec. VII. Finally, in Sec. VIII, we conclude this work considering what more must be explored.

II. RELATED WORKS

A. The THz Channel

The propagation loss of a wireless signal is characterized by the Friis path loss equation. These losses occur due to the fact that signals propagate radially outward in every direction from an isotropic antenna, and they depend heavily on the antenna's surface area. The size of the antenna is directly proportional to the signal wavelength. Thus THz signals, with wavelengths on the order of hundreds to thousands of micrometers, suffer significant propagation losses compared to lower frequency signals. In addition to propagation losses, THz signals also experience absorption losses. Air molecules - specifically water vapor molecules - have resonances at THz frequencies. As a result, when THz signals are radiated through the air, these molecules are excited and absorb some of the radiated energy [8]. This absorption results in a reduced amplitude of the signal at the receiver and contributes to the overall path loss in addition to propagation loss from the Friis path loss equation. Thus, the total path loss in the THz band is the combination of absorption and spreading losses and is given by

$$L = \left(\frac{4\pi fr}{c}\right)^2 e^{kr},\tag{1}$$

where f is the carrier frequency, c is the speed of light, k is the frequency-dependent molecular absorption constant, and r is the transmission distance. The spreading losses accounts for most of the loss seen in the THz band, especially considering that absorption losses only exist at the specific resonant frequency of water vapor molecules. This results in a frequency selective channel in which there are large absorption-free windows between the resonant frequencies of water vapor. In these pockets of bandwidth, absorption loss can be negligible. As signals propagate farther, however, they encounter more air molecules, which results in more absorption losses. Thus absorption lines broaden with distance, causing the absorption-free windows to shrink [8]. Fig. 1 shows the path loss as a function of frequency. The different colored lines correspond to various transmission distance. As mentioned, the absorption lines broaden as the transmission distance increases, and in between those lines, windows of absorption-free bandwidth are labeled.

The high path loss and the distance-dependent bandwidth caused by molecular absorption should motivate how the physical layer is designed for THz communication systems. Specifically traditional STMR systems with receivers at different distances, the aggregate achievable capacity is limited by the the smallest available bandwidth.

B. Related Solutions

Numerous hardware solutions have been presented to combat the path loss problem in the THz band. One of the most common is the use of directional antennas such as horn antennas [9]. With a directional antenna, the effective area of the antenna is increased leading to smaller path loss. Although often a useful solution, directional antennas are not always practical. For instance, in mobile applications, directional antennas would require mechanical steering. Moreover, in the event that a directional antenna does not provide sufficient gain, additional measures would be needed in order to ensure system performance.

Considering these challenges multiple-input multiple-output (MIMO) and ultra-massivie MIMO (UM-MIMO) have been introduced for THz communications to allow for digital or analog beam steering, high directionality, and combining gains if a line-of-sight (LoS) component is weak or unavailable [10]. Despite these developments, there are scenarios in which MIMO systems would likely need to be supplemented by THz signal reflecting mirrors [11] or intelligent reflecting surfaces [12]. These solutions propose installing filters and reflectors for THz signals to create an environment that promotes better propagation for a THz communication system.

Although many results have been presented for these hardware solutions in THz communications, only a few solutions have considered the signal waveform itself as an opportunity to address or exploit the THz channel's unique properties. The authors of [13] exploit the THz band's high loss to ensure covertness and security. Due to the THz channel they suggest deliberately transmitting at the resonances of water vapor to prevent eavesdropping. Although useful for covert communications, this solution does not allow for farther or faster transmissions.

In [14] and [15] the authors present Distance Aware Multi-Carrier (DAMC) Modulation, an approach to allocate frequency sub-carriers in a multi-user system according to users' available bandwidth. In this approach, users closer to the transmitter (i.e. experiencing less absorption) are allocated frequency sub-carriers closer to absorption lines while users farther away from the transmitter (i.e. experiencing more absorption) use frequency sub-carriers far away from absorption lines. This work was expanded on in [16] and [17] to propose dynamically adjust sub-carriers to accommodate the THz channel's distance-dependent characteristics. DAMC offers a useful way to work around absorption losses but does not exploit the absorption losses or offer a solution for high propagation loss situations that are not a result of absorption.

A similar approach is shared in [18], where the authors present an orthogonal frequency division multiplexing (OFDM) scheme that evaluates subcarriers' bandwidth, power allocation, and modulation order while considering the frequency selectivity of the channel. This scheme is more

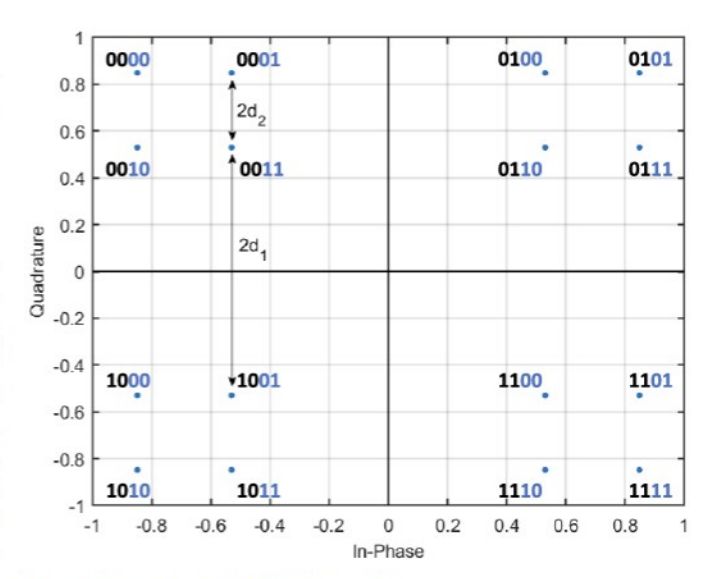


Fig. 2. Hierarchical 4/16-QAM Constellation.

spectrally efficient than DAMC and requires less complexity for the transmitter, but still does not leverage the THz channel's distance-dependent bandwidth as an advantage.

Another proposed method is to use chirp modulated phase shift keying (PSK) symbols to transmit across molecular absorption lines [19]. In this approach, the transmitted chirp signal includes multiple frequencies, so even in the presence of an absorption line, the receiver should still be able to identify the symbol based on the frequencies that have not been absorbed by water vapor. Although a creative and effective solution, similar to DAMC, the chirp signal does not leverage the THz channel's unique characteristics as an advantage or offer a solution for high propagation loss across a range of frequencies.

Traditional HM [20], [21] is a modulation scheme for STMR systems that employs a hierarchical constellation. It was presented for broadcast backwards compatible digital television systems [22], has been optimized for RF broadcast scenarios [23], and has recently been used for millimeter wave communications [24]. A similar concept can offer the flexibility and higher aggregate data rates we desire for the THz band. In traditional HM, receivers that observe a higher signal-tonoise ratio (SNR) demodulate a higher order constellation than users with a lower SNR [20].

An example of a 4/16-QAM hierarchical constellation is shown in Fig. 2. Notice that the points are not equidistant from each other. If a system were to use the multi-resolution 4/16-QAM shown in Fig. 2 receivers experiencing a high SNR would demodulate each of the 16 individual constellation points. Meanwhile, receivers farther away experiencing a lower SNR would only demodulate the 4-QAM corresponding to the four-point clusters in each quadrant. Thus, these receivers would see a lower resolution of information. In a THz communications context, this flexibility for receivers with respect to SNR allows users to adjust to their perceived channel while still successfully demodulating necessary information. However, traditional HM does not

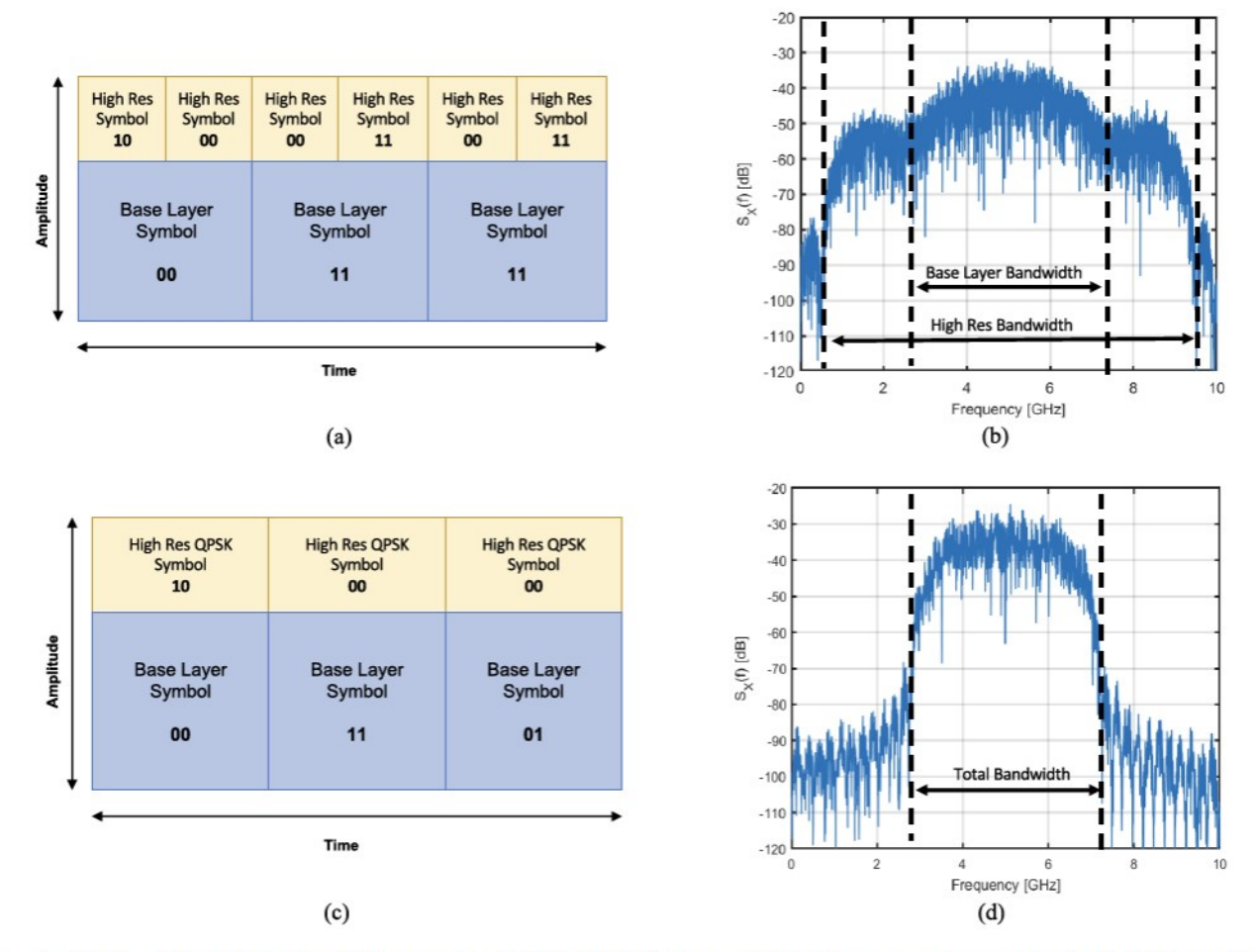


Fig. 3. Amplitude and Time Distribution of (a) an example 4/16-QAM HBM System and (b) its frequency spectrum compared with (c) the amplitude and time distribution of a traditional 4/16-QAM HM System and (d) its frequency spectrum.

consider the distance-dependent bandwidth of the THz channel into account.

III. HIERARCHICAL BANDWIDTH MODULATIONS A. What is HBM?

An HBM system uses a hierarchical constellation similar to HM, but HBM also introduces a hierarchy in bandwidth and therefore in the symbol duration as well. The differences between a HM and HBM signal are shown in Fig. 3a and Fig. 3c.

Although both the HM symbols and HBM symbols contain base level of information (the blue symbols) sent with a larger amplitude than the secondary information symbols (the yellow symbols), the HBM high resolution symbols occur at twice the rate as those for HM. Thus, HBM can achieve faster aggregate data rates. This hierarchy in bandwidth can also be seen in the signal spectrum itself. Fig. 3b and Fig. 3d show the baseband spectrum of an HBM and traditional HM signal respectively. The HBM signal has a high resolution bandwidth of 10 GHz and a low resolution bandwidth of 5 GHz. The low resolution bandwidth is seen as a main lobe from 2.5-7.5 GHz, and on either side of it there are smaller lobes bringing the entire high resolution bandwidth from 0-10 GHz. These additional lobes on either side of the

main lobe do not contain any low resolution information, and a low resolution system would not see them. In fact if the low resolution receiver could see them at all, it would likely filter them out using a band pass filter. Even without those portions of the signal, the low resolution receiver would still receive a full lobe of bandwidth information due to the hierarchical design of the signal. The corresponding HM spectrum only has one main lobe corresponding to the smaller bandwidth; its hierarchy only exists in amplitude whereas for HBM there is also a hierarchy in bandwidth and in time. The frequency spectrums shown in Fig. 3b and Fig. 3d also show that HBM can use an overall broader bandwidth than traditional HM can use, which enables HBM to achieve the higher aggregate data rate.

This hierarchy in bandwidth is useful in the THz band, especially if the transmission is close to an absorption line. The channel between the transmitter and users at farther transmission distances will filter out the high resolution sidelobe(s). When absorption is not present, HBM can still improve performance by allowing users with a lower SNR to use a smaller bandwidth and therefore reduce the observed noise power. Furthermore, although we focus on the LoS scenario, non-LoS and multi-path channels are being explored for THz communications [25], [26]. In the LoS case in the presence of

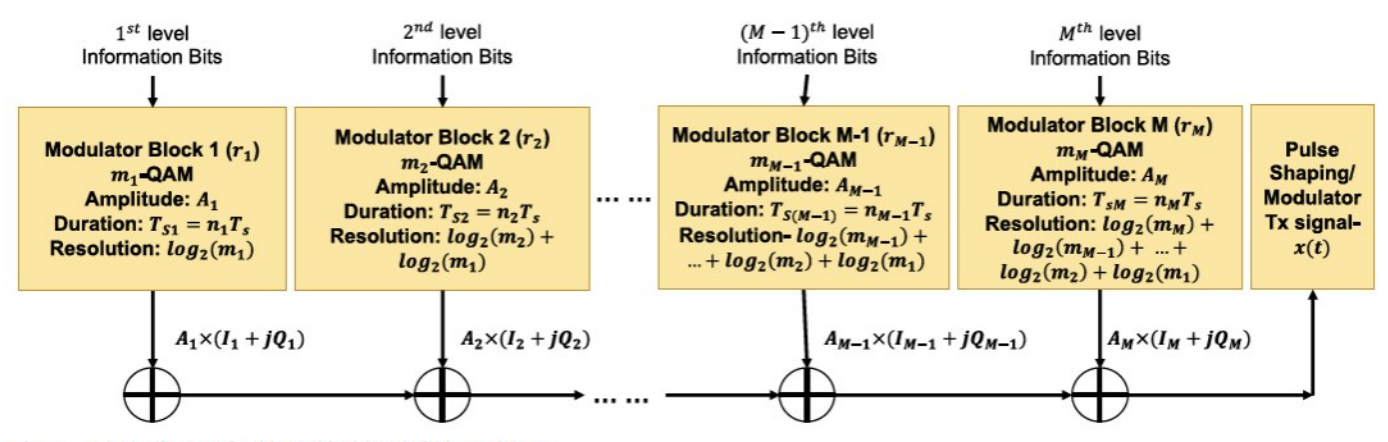


Fig. 4. Block diagram for hierarchical bandwidth modulator.

multi-path, the multi-path components are traveling a longer distance than the LoS, which will result in the absorption lines filtering part of the signal. In the case where the primary path is a non-LoS path, HBM analysis is still valid as long as the total path length is considered.

B. Modulator Design

In order for this modulation scheme to work, the adjacent high resolution HBM symbols within one low resolution symbol shown in Fig. 3 must exist within the same cluster of the constellation shown in Fig. 2. This interrelation can be achieved by using the block-wise modulator in Fig. 4. Each block represents a corresponding level of resolution in the constellation and in time. The symbol duration for the modulator block 1, 2, ...M is given by $T_{s1} = n_1 T_s, T_{s2} =$ $n_2T_s,\ldots,T_{sM}=n_MT_s$, respectively. Here, T_s is the base symbol duration, and $\frac{n_1}{n_2}, \frac{n_2}{n_3}, \dots, \frac{n_{M-1}}{n_M}$ should all be integers. Thus the number of transmitted bits per the base symbol time are given by $\frac{\log_2(m_1)}{n_1} + \frac{\log_2(m_2)}{n_2} + \ldots + \frac{\log_2(m_M)}{n_M}$. The total modulation order achieved after level M is $m_T =$ $m_1 \times m_2 \times \dots m_M$, where m_i is the modulation index for the ith modulator block. For efficient utilization of HBM in terms of bandwidth usage the ratio would often be 2, which implies $\frac{T_{S1}}{T_{S2}} = \frac{n_1}{n_2} = 2$. This indicates that for fixed transmission power, higher level modulations are held for shorter times, resulting in a lower energy per bit E_b . However, over the shorter distances at which these symbols are expected to be received, the channel path loss is lower which results in higher E_b/N_o values at these receivers.

The m_i -QAM constellation at each block is scaled by A_i such that $A_1 > A_2 > ... A_M$ and such that $\sum_{m=1}^M A_m$ satisfies the system energy requirements. It is also important to choose the amplitudes such that constellation points from subsequent modulators do not overlap. This can be achieved using the conditions given by

$$\frac{A_1}{(\sqrt{m_1} - 1)} \ge A_2 + A_3 + \dots A_M,\tag{2}$$

$$\frac{A_1}{(\sqrt{m_1} - 1)} \ge A_2 + A_3 + \dots A_M,$$

$$\frac{A_2}{(\sqrt{m_2} - 1)} \ge A_3 + A_4 + \dots A_M,$$
(2)

$$\frac{A_{M-1}}{\left(\sqrt{m_{M-1}}-1\right)} \ge A_M. \tag{4}$$

These amplitude values and the constellation orders of each block generate a hierarchical constellation. To generate a hierarchy in bandwidth, each block operates with a different symbol duration.

The bits at each block are mapped to required I and Q symbols within the m_i -QAM constellation. Thus the transmitted I and Q values for the highest resolution symbol time can be represented by

$$I + jQ = A_1(I_1 + jQ_1)$$

 $+A_2(I_2 + jQ_2) + \dots \cdot A_M(I_M + jQ_M),$ (5)

where $I_1 + jQ_1, I_2 + jQ_2, \dots I_M + jQ_M$ are normalized I and Q components generated by the modulator blocks 1 though M. In the next instance of T_{sM} , $I_1 + jQ_1$, $I_2 + jQ_2$, ... $I_{M-1} +$ jQ_{M-1} would be held constant while the M^{th} modulation block would produce a new $I_M + jQ_M$ symbol. In the following T_{sM} time instance, $I_1 + jQ_1, I_2 + jQ_2, ... I_{M-2} + jQ_{M-2}$ would be held constant while the M^{th} and $M-1^{th}$ modulation blocks would produce a new symbols and so on.

Thus the base I and Q symbols generated at 1st modulator block are intended for all receivers. They have the lowest resolution symbols in terms of the constellation and occupy the longest symbol duration (i.e., smallest bandwidth). The higher resolution symbols are modulated on top of the base modulation for the closer receivers. Therefore, the end modulator block modulates the symbol based on all the previous modulators and has the shortest symbol duration (i.e., largest bandwidth). The modulator output signal is based on a bitstream that is the combination of the bits from each modulator block, and at the end of the block-wise modulator, the signal is shaped with the highest resolution I and Q symbols by a pulse shaping block.

On the receiver side, the signal is demodulated according to the SNR and bandwidth observed at the receiver to maintain a low SER. Therefore, in LoS communication, the farthest receiver with the lowest SNR and narrowest bandwidth would demodulate the base or low-resolution bitstream, and the closest receiver with the highest SNR and bandwidth have the highest-resolution demodulating capability. We focus on LoS communications in this paper only because it allows for simple estimation of the receivers' SNRs and bandwidths. As long as

receivers are able to evaluate their bandwidth and received SNR, HBM would also work in non-LoS scenarios.

An example of a two-level HBM encoding scheme was shown in Fig. 2. In that case, both m_1 and m_2 were set to 4, resulting in a non-uniform 16-QAM for the highest level of resolution. Hence the name of the HBM scheme is 4/16-QAM. The first pair of bits, corresponding to the base layer information, were given a certain amplitude and held for the symbol time T_S ($n_1=1$). The following two pairs of bits corresponding to high-resolution information were given a smaller amplitude, and each held for time $\frac{1}{2}T_S$ ($n_2=\frac{1}{2}$) in succession.

Even though we focus on QAM constellations here, multiresolution constellations can come in a variety shapes and sizes [20], and any hierarchical constellation would work for HBM. Going forward, we focus on the two-level HBM scheme, where the base or first level modulation is the 4-QAM and the second level modulation is M-QAM. The results, such as constellation design, theoretical SER calculation, obtained from the two-level system can be extended for the higher-level schemes and higher-order modulations.

IV. ERROR RATE PERFORMANCE

In this section we characterize HBM's SER performance by deriving the expected error rates for the 4/16-QAM and 4/M-QAM HBM system.

The constellation diagram for the 4/16-QAM system was shown in Fig. 2 along with the variables d_1 and d_2 . d_1 is the distance from the In-Phase or Quadrature axis to the closest symbol and $2d_2$ is the minimum distance between two high resolution symbols. λ is defined as the ratio of $\frac{d_2}{d_1}$ which helps characterize the ratio of power used for the high resolution and low resolution information. These will be key parameters in finding the SER as a function of $\frac{E_2}{N_0}$.

For the closer or high resolution receiver, the constellation looks like a non-uniform 16-QAM and the resulting SER can be derived considering the 16-QAM as the Cartesian product of a one dimensional 4-PAM constellation with itself [27]. The corresponding non-uniform 4-PAM constellation is shown in Fig. 5. Considering equally probable symbols, the likelihood of symbol error for the non-uniform 4-PAM constellation shown is given by:

$$P_e = Q\left(\frac{d_2}{\sqrt{\frac{N_0}{2}}}\right) + \frac{1}{2}Q\left(\frac{d_1}{\sqrt{\frac{N_0}{2}}}\right),$$
 (6)

where Q(.) is the standard Q-function. This expression can be used to find the probability of correct detection for the corresponding 16-QAM

$$P_c = (1 - P_e)^2. (7)$$

Hence, the probability of symbol error for 16-QAM is

$$SER_{HighRes} = 1 - P_c \approx 2P_e = 2Q \left(\frac{d_2}{\sqrt{\frac{N_0}{2}}}\right) + Q \left(\frac{d_1}{\sqrt{\frac{N_0}{2}}}\right),$$
(8)



Fig. 5. Constellation diagram for the non-uniform 4PAM modulation.



Fig. 6. Constellation diagram for the non-uniform 6-PAM modulation observed by low resolution receiver.

where $SER_{HighRes}$ is the probability of symbol error for the closer receiver demodulating the high resolution constellation.

The low resolution SER expression calculated for traditional HM in [21] offers a consistent upper bound for the low resolution HM receiver. It is given by

$$SER_{LowRes} = Q\left(\frac{d_1 + 2d_2}{\sqrt{\frac{N_0}{2}}}\right) + Q\left(\frac{d_1}{\sqrt{\frac{N_0}{2}}}\right). \tag{9}$$

To find a tighter bound for HBM, we must consider what exactly the corresponding low resolution receiver will observe, which is different from an HM receiver. The same 16-QAM constellation that was used for the high resolution receiver is transmitted, but the low resolution receiver operates with a longer symbol duration (i.e. smaller bandwidth). Thus, instead of considering one symbol at a time, the low resolution receiver demodulates $\frac{n_1}{n_2}$ consecutive high resolution symbols at once. These symbols exist in the same quadrant of Fig. 2. For efficient utilization of the bandwidth, we take $\frac{n_1}{n_2} = 2$ for low resolution symbols that are twice as long as the high resolution symbols. Thus, unlike the high resolution case, which corresponds to the non-uniform 4-PAM in Fig. 5, the low resolution receiver observes the transmitted constellation as binary PAM with the three distinct points on each shown in Fig. 6. In the case of consecutive transmission of two identical high resolution symbols, the receiver detects the constellation points on one of the grey points. Whereas for the case of transmission of two different high resolution symbols (i.e., symbol at d_1 and $d_1 + 2d_2$ for PAM system on I/Q axis) within one low resolution symbol duration, the middle point is detected by the low resolution receiver as an average value, i.e, $d_1 + d_2$ denoted by the yellow points. These points are not truly being transmitted but are the observed constellation point when an outer and inner point are transmitted within one low resolution symbol time. Therefore, the error probability for the low resolution receiver is given by

$$P_{e} = \frac{2}{8} \left(Q \left(\frac{d_{1} + 2d_{2}}{\sqrt{\frac{N_{0}}{2}}} \right) + Q \left(\frac{d_{1}}{\sqrt{\frac{N_{0}}{2}}} \right) + 2Q \left(\frac{d_{1} + d_{2}}{\sqrt{\frac{N_{0}}{2}}} \right) \right), \tag{10}$$

where $Q\left(\frac{d_1+2d_2}{\sqrt{\frac{N_0}{2}}}\right)$ is the probability that an outer edge symbol is received in error, $Q\left(\frac{d_1}{\sqrt{\frac{N_0}{2}}}\right)$ is the probability

an inner symbol is received in error, and $Q\left(\frac{d_1+d_2}{\sqrt{\frac{N_0}{2}}}\right)$ is the probability a yellow symbol is received in error. We multiply by 2 to account for symbols on either side of the origin, and we divide by 8 because there are 8 possible pairs of high resolution symbols that are transmitted within a low resolution symbol.

Using (7) again and recalling that $\lambda = \frac{d_2}{d_1}$ the expression for the low and high resolution error rates can be rewritten in terms of d_1 and λ which gives us

$$SER_{LowRes} = \frac{1}{2} \left(Q \left(\frac{d_1(1+2\lambda)}{\sqrt{\frac{N_0}{2}}} \right) + Q \left(\frac{d_1}{\sqrt{\frac{N_0}{2}}} \right) + 2Q \left(\frac{d_1(1+\lambda)}{\sqrt{\frac{N_0}{2}}} \right) \right)$$
(11)

and

$$SER_{HighRes} = 2Q\left(\frac{d_1\lambda}{\sqrt{\frac{N_0}{2}}}\right) + Q\left(\frac{d_1}{\sqrt{\frac{N_0}{2}}}\right)$$
 (12)

for the low and high resolutions respectively. The average symbol energy can be found from Fig. 2 in terms of d_1 and d_2 to be

$$E_s = \frac{1}{16} \left(4(2d_1^2) + 8(d_1^2 + (d_1 + 2d_2)^2) + 4(2(d_1 + 2d_2)^2) \right). \tag{13}$$

Simplifying, substituting $d_2 = \lambda d_1$, and rearranging, we find

$$d_1 = \sqrt{\frac{E_s}{2(1+2\lambda+2\lambda^2)}}. (14)$$

Using this expression in (12) the symbol error rate as a function of $\frac{E_s}{N_0}$ for the low resolution receiver is determined to be

$$SER_{LowRes} = \frac{1}{2}Q\left((1+2\lambda)\sqrt{\frac{\frac{E_{s}'}{N_{0}}}{1+2\lambda+2\lambda^{2}}}\right) + Q\left(\sqrt{\frac{\frac{E_{s}'}{N_{0}}}{1+2\lambda+2\lambda^{2}}}\right) + 2Q\left((1+\lambda)\sqrt{\frac{\frac{E_{s}'}{N_{0}}}{1+\lambda+2\lambda^{2}}}\right).$$
(15)

While for the high resolution receiver it is given by

$$SER_{HighRes} = 2Q \left(\lambda \sqrt{\frac{\frac{E_s}{N_0}}{1 + 2\lambda + 2\lambda^2}} \right) + Q \left(\sqrt{\frac{\frac{E_s}{N_0}}{1 + 2\lambda + 2\lambda^2}} \right). \quad (16)$$

For the low resolution receiver, we use E'_s to indicate that the symbol energy in order to differentiate it from the high resolution receiver's symbol energy. $E'_s = E_s \frac{n_1}{n_2}$ because the

low resolution symbols are held $\frac{n_1}{n_2}$ times longer than the high resolution symbols. We emphasize again that in our simulations and calculations, we take $\frac{n_1}{n_2}=2$ for low resolution symbols that are twice as long as the high resolution symbols. Decreasing the value of n_2 corresponds to including more high resolution symbols in each low resolution symbol. This would result in additional yellow symbols between the inner and outer constellation points in Fig. 6, essentially reducing the probability that the outer- and inner-most constellation points are observed by the low resolution receiver. Thus we can infer that decreasing n_2 would improve the low resolution receiver's performance.

For the 4/M-QAM case, the high and low resolution expected error rates can be derived similarly. The parameters are the same as they were for the 4/16-QAM case, and there are now more points in the high resolution portion of the constellation. d_1 and d_2 still characterize the amount of power used for the low and high resolution information respectively, and λ is still used to represent the ratio $\frac{d_2}{d_1}$. The base non-uniform PAM constellation shown in Fig. 8 can be extrapolated to create the 4/M-QAM constellation shown in Fig. 7.

The full derivation is given in appendix A, but the resulting error rates are given by (17) and (18), shown on the next page.

V. PERFORMANCE ANALYSIS

In this section, we explore the error rates' dependence on transmission distance and λ , and we proceed to show that HBM thoroughly outperforms traditional HM in terms of the aggregate data rate.

A. Performance Dependence on Transmission Distance and λ

From the error rates derived in Sec. IV, it is interesting to note that the $\frac{E_s}{N_0}$ for each HBM receiver depends on both λ and the transmission distance. All transmitters have finite peak power at which they can transmit, and because increasing λ spreads out the constellation, the average symbol energy will decrease as λ increases. The symbol energy also decreases as the distance increases simply due to the spreading losses. This relation is shown in Fig. 9a. As the distance increases the ratio $\frac{E_s}{N_0}$ seen at the receiver decreases for all values of λ . However, this decrease is slightly less when λ is smaller.

From this result we can also find the SER as a function of λ and the transmission distance as shown in Fig. 9b. As expected, both error rates increase with distance. The low resolution error rate also increases with λ while the high resolution error rate decreases as λ approaches 1.

It is also important to remember that a high resolution HBM receiver will have a smaller $\frac{E_a}{N_0}$ value than a HM receiver at the same distance due to its shorter symbol duration (i.e. larger bandwidth). Thus, for a given SER threshold, HM can successfully transmit using a higher order constellation for the high resolution receivers, but HBM will be transmitting symbols to high resolution receivers at a faster rate. This phenomenon is shown in Fig. 10. The $\frac{E_a}{N_0}$ of the HM high resolution receiver is shown on the x-axis while the bit error rates (BERs) for the various HM and HBM 4/M-QAM schemes are plotted on the y-axis for different values of λ .

Looking at the 4/16-QAM HBM constellation as an example, we see that its performance is comparable to that of the 4/64-QAM HM constellation. Similarly, 4/64-QAM HBM constellation has a comparable performance to the 4/256-QAM HM constellation's performance. This is especially the case for smaller values of λ . From these relations we can see that, for the same transmit power and transmission distance, an HBM system must use a lower order constellation for its high resolution information in order to achieve the same performance as a corresponding HM system. Thus we proceed to investigate whether HBM actually improves the aggregate data rate compared to traditional HM.

B. HBM v. HM Aggregate Data Rates

To find the aggregate data rates of the HM and HBM systems we use the following expression

$$R = \frac{\log_2(M_L)}{T_{s1}} + \frac{\log_2(M_H)}{T_{s2}},\tag{19}$$

where M_H and M_L are the high and low resolution modulation order respectively, and for traditional HM $T_{s1}=T_{s2}=nT_s$. T_s is the shortest possible symbol time determined by the bandwidth. For HBM, M_H and M_L are still the high and low resolution modulation order respectively, but $T_{s1}=n_1T_s$ and $T_{s2}=n_2T_s$, where $\frac{n_1}{n_2}$ is an integer, we take to be 2.

To evaluate which system would truly transmit at the fastest data rate, we use a full end-to-end simulation to represent a STMR system operating at 120 GHz with receivers at 3m and 30m. These receivers observe $\frac{E_s}{N_0}$ values of 14dB and 37dB respectively for HM and 14dB and 34dB for HBM. The symbol rate for the low resolution receivers will be the same for both HM and HBM, but the symbol rates for the high resolution receivers and the aggregate data rates will differ. With 5 GHz of bandwidth visible for both the high and low resolution receivers, the HM system can use a 4/256-QAM while keeping its uncoded error rate below 10^{-3} . The bit rate for the high resolution receiver is

$$SER_{HighRes} = \frac{4}{\sqrt{M}} \left(\left(\sqrt{M} - 2 \right) \right) \times Q \left(\lambda \sqrt{\frac{E_s}{N_0}} \frac{M}{4 \sum_{i=0}^{\frac{\sqrt{M}}{2} - 1} \sum_{j=0}^{\frac{\sqrt{M}}{2} - 1} (1 + 2i\lambda + 2j\lambda + 2i^2\lambda^2 + 2j^2\lambda^2)} \right) + Q \left(\sqrt{\frac{E_s}{N_0}} \frac{M}{4 \sum_{i=0}^{\frac{\sqrt{M}}{2} - 1} \sum_{j=0}^{\frac{\sqrt{M}}{2} - 1} (1 + 2i\lambda + 2j\lambda + 2i^2\lambda^2 + 2j^2\lambda^2)} \right),$$
(17)

 SER_{LowRes}

$$\begin{split} &=\frac{8}{M}\bigg[Q\left(\sqrt{\frac{E_s'}{N_0}}\frac{M}{4\sum_{i=0}^{\frac{\sqrt{M}}{2}-1}\sum_{j=0}^{\frac{\sqrt{M}}{2}-1}(1+2i\lambda+2j\lambda+2i^2\lambda^2+2j^2\lambda^2)}\right)\\ &+Q\left(\left(2\left(\frac{\sqrt{M}}{2}-1\right)\lambda+1\right)\sqrt{\frac{E_s'}{N_0}}\frac{M}{4\sum_{i=0}^{\frac{\sqrt{M}}{2}-1}\sum_{j=0}^{\frac{\sqrt{M}}{2}-1}(1+2i\lambda+2j\lambda+2i^2\lambda^2+2j^2\lambda^2)}\right)\\ &+\frac{\sqrt{M}}{2}Q\left(\left(\left(\frac{\sqrt{M}}{2}-1\right)\lambda+1\right)\sqrt{\frac{E_s'}{N_0}}\frac{M}{4\sum_{i=0}^{\frac{\sqrt{M}}{2}-1}\sum_{j=0}^{\frac{\sqrt{M}}{2}-1}(1+2i\lambda+2j\lambda+2i^2\lambda^2+2j^2\lambda^2)}\right)\\ &+\sum_{n=1}^{\left(\frac{\sqrt{M}}{2}+1\right)\frac{1}{2}}\left\{\left((2n-1)+1\right)\left(Q\left(\left((2n-1)\lambda+1\right)\sqrt{\frac{E_s'}{N_0}}\frac{M}{4\sum_{i=0}^{\frac{\sqrt{M}}{2}-1}\sum_{j=0}^{\frac{\sqrt{M}}{2}-1}(1+2i\lambda+2j\lambda+2i^2\lambda^2+2j^2\lambda^2)}\right)\\ &+Q\left(\left((2n-1)+1\right)\lambda+1\right)\sqrt{\frac{E_s'}{N_0}}\frac{M}{4\sum_{i=0}^{\frac{\sqrt{M}}{2}-1}\sum_{j=0}^{\frac{\sqrt{M}}{2}-1}\left(1+2i\lambda+2j\lambda+2i^2\lambda^2+2j^2\lambda^2\right)}\right)\\ &+Q\left(\left(\left(\frac{\sqrt{M}}{2}-1+(2n-1)\right)\lambda+1\right)\sqrt{\frac{E_s'}{N_0}}\frac{M}{4\sum_{i=0}^{\frac{\sqrt{M}}{2}-1}\sum_{j=0}^{\frac{\sqrt{M}}{2}-1}\left(1+2i\lambda+2j\lambda+2i^2\lambda^2+2j^2\lambda^2\right)}\right)\\ &+Q\left(\left(\left(\frac{\sqrt{M}}{2}-1+(2n-1)\right)\lambda+1\right)\sqrt{\frac{E_s'}{N_0}}\frac{M}{4\sum_{i=0}^{\frac{\sqrt{M}}{2}-1}\sum_{j=0}^{\frac{\sqrt{M}}{2}-1}\left(1+2i\lambda+2j\lambda+2i^2\lambda^2+2j^2\lambda^2\right)}\right)\\ &+Q\left(\left(\left(\frac{\sqrt{M}}{2}-1+(2n-1)+1\right)\lambda+1\right)\sqrt{\frac{E_s'}{N_0}}\frac{M}{4\sum_{i=0}^{\frac{\sqrt{M}}{2}-1}\sum_{j=0}^{\frac{\sqrt{M}}{2}-1}\left(1+2i\lambda+2j\lambda+2i^2\lambda^2+2j^2\lambda^2\right)}\right)\right)\right]. \end{split}$$

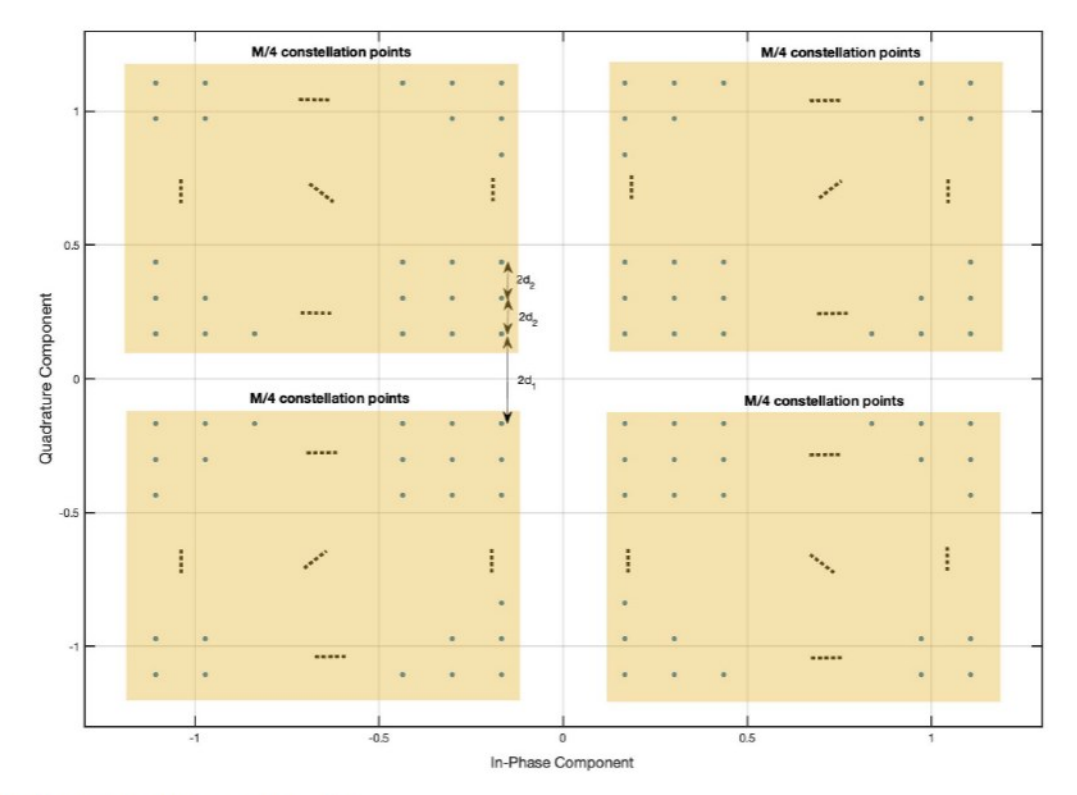


Fig. 7. 4/M-QAM Constellation Diagram with $\lambda = \frac{d_2}{d_1}$.



Fig. 8. Constellation diagram for the non-uniform PAM modulation for the 4/M-QAM constellation.

given by

$$R_{HighRes} = \log_2(M_{HighRes}) * \frac{B_{HighRes}}{2},$$
 (20)

where $M_{HighRes}$ is the highest order of modulation, 256 in this case, and the signal bandwidth B is two times the symbol rate. Thus in the described HM system, the symbol rate is 2.5 Gsps, and the bit rate is 20 Gbps for the high resolution receiver. The low resolution receiver's bit rate is very similar, given by

$$R_{LowRes} = \log_2(M_{LowRes}) * \frac{B_{LowRes}}{2}.$$
 (21)

In the case of traditional HM, $B_{HighRes} = B_{LowRes}$.

An HBM receiver using the same set-up has the same 5 GHz of bandwidth for the low resolution receiver, but the high resolution receiver has a bandwidth of 10 GHz, corresponding to a symbol rate of 5 Gsps. Due to its larger bandwidth, this receiver experiences more noise and is therefore only able to operate with a 4/64-QAM while maintaining the same uncoded error rate threshold of 10⁻³. Using equation (20), the bit rate is found to be 30 Gbps. The low resolution receiver's bit rate is calculated from (21) and is the same as that of the traditional HM low resolution receiver: 5 Gbps.

The aggregate data rates for each STMR system are found by adding the high and low resolution data rates

$$R_{Agaregate} = R_{LowRes} + R_{HighRes},$$
 (22)

and Fig. 11a displays the results obtained in this example. The HM system has an aggregate rate of 25 Gbps while HBM has an aggregate data rate of 35 Gbps. Thus, even though the constellation order is smaller, HBM outpaces traditional HM in terms of data rate while achieving the same error rate performance. In other words, even though HM uses a constellation order of 256 for the high resolution receiver, HBM achieves a data rate 10 Gbps higher than that of HM while experiencing a comparable error rate. This is possible because HBM uses a faster symbol rate for the high resolution information. A similar result is shown for higher orders of M and larger bandwidths that would truly take advantage of the THz band's availability in Fig. 11b. In this example, the low resolution receivers would require an $\frac{E_s}{N_0}$ of at least 14 dB while the HM and HBM high resolution receivers would require $\frac{E_s}{N_0}$ values of 31 dB and 25 dB respectively. Despite using a lower modulation order and requiring a smaller $\frac{E_s}{N_o}$, HBM reaches an aggregate rate above 1 Tbps before HM by exploiting the distance-dependent bandwidth available in the THz band.

VI. THE HBM FUNCTIONAL REGION

In this section we define the HBM functional region and consider its significance when designing static systems as well as systems with varying channel characteristics. We proceed

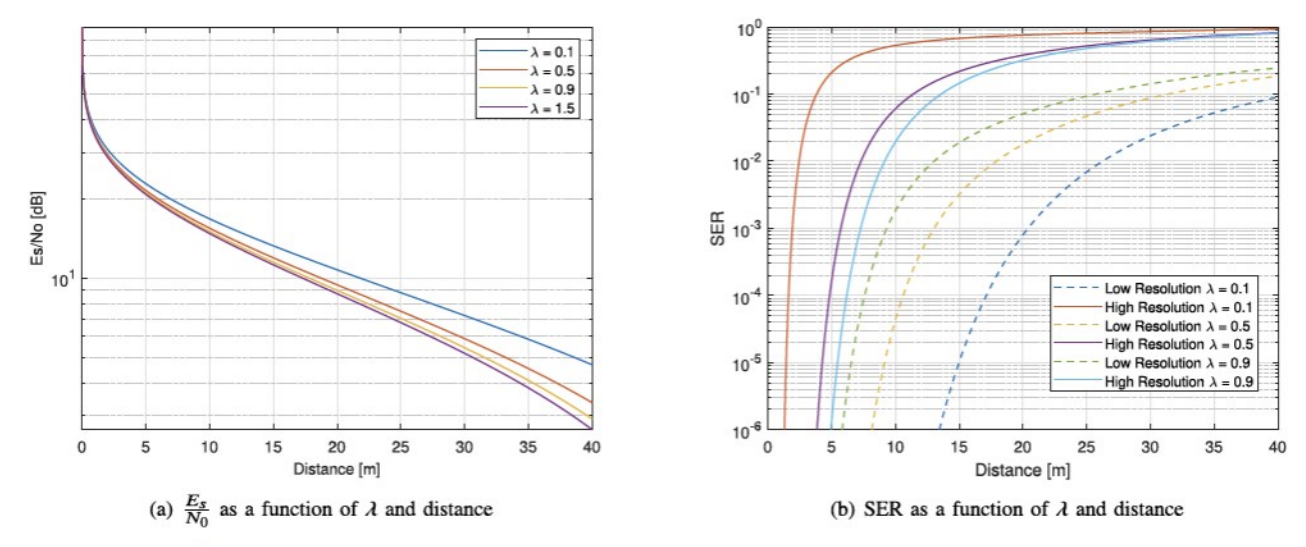


Fig. 9. HBM receiver's $\frac{E_s}{N_0}$ and SER dependence on λ and transmission distance.

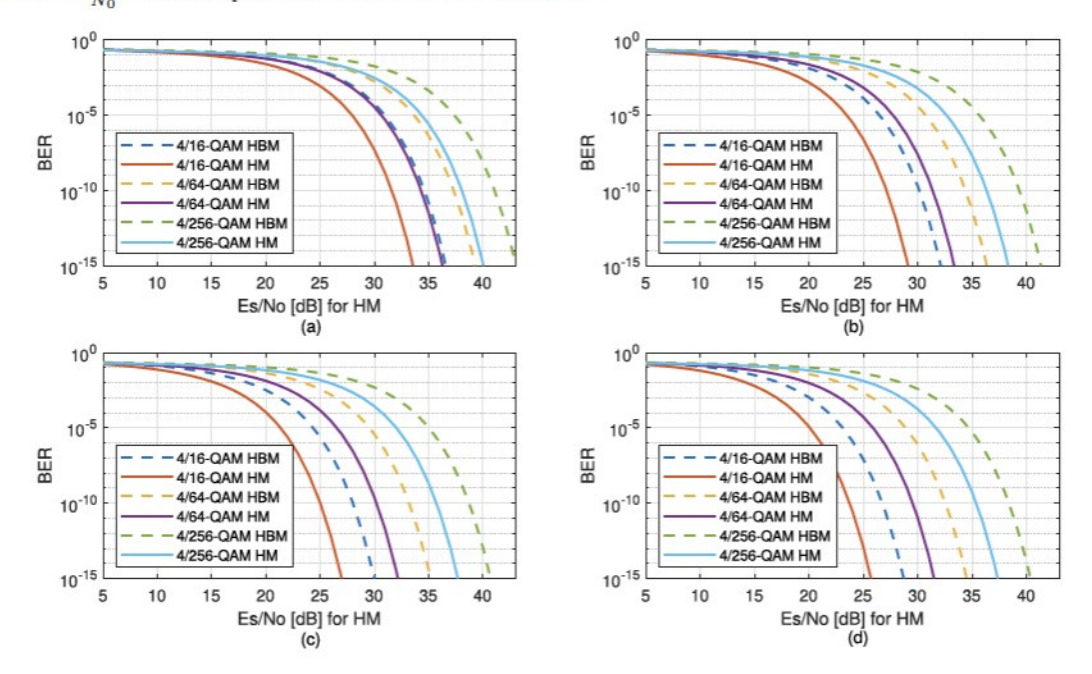


Fig. 10. A comparison of the high resolution error rates of HM and HBM for (a) $\lambda = 0.2$, (b) $\lambda = 0.4$, (c) $\lambda = 0.6$, (d) $\lambda = 0.8$.

to experimentally verify the existence of the experimental functional region.

A. What is the HBM Functional Region?

Now that the SER's dependence on $\frac{E_s}{N_0}$ and λ has been fully characterized, the SER can be represented as a function of λ and transmission distance. Thus, for a pair of distances, the expected $\frac{E_s}{N_0}$ can be found as a function of λ . Then, given a maximum SER threshold, the necessary range of λ s to maintain an SER below the threshold can be found. In other words, to design a functional HBM system, we can determine the range of λ such that

$$SER_{HighRes}\left(\frac{E_s}{N_0},\lambda\right) < SER_{Th} \cap SER_{LowRes}\left(\frac{E_s'}{N_0},\lambda\right) < SER_{Th}$$
 (23)

where SER_{Th} is the threshold SER and $\frac{E_s}{N_0}$ values are determined using a link budget analysis for the transmission distances. We call the range of λ values which satisfy (23) the HBM functional region. As an example, the scenario of two stationary receivers at 3m and 12m in a 4/16-QAM HBM system is considered. To find the functional region, the expected $\frac{E_s}{N_0}$ values for the experimental system is calculated for 3m and 12m, and the SER is calculated as a function of lambda for each receiver. The results are shown in Fig. 12. The SER curves for each resolution follow what intuition would expect. For the low resolution receiver, the SER is minimized when λ is equal to 0. This corresponds to the uniform 4-QAM that the low resolution receiver is trying to demodulate. From the low resolution receiver's perspective, increasing λ increases unwanted deviations from the base layer symbols, thus when these deviations do not occur, the low resolution receiver demodulates at its best. Conversely,

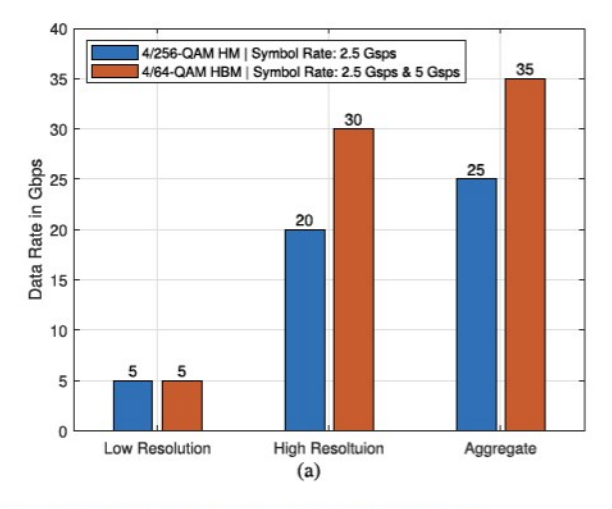


Fig. 11. Achievable data rates for HM and HBM systems.

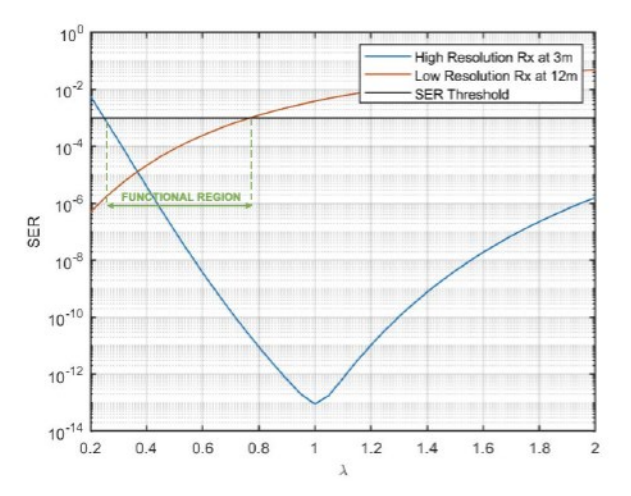
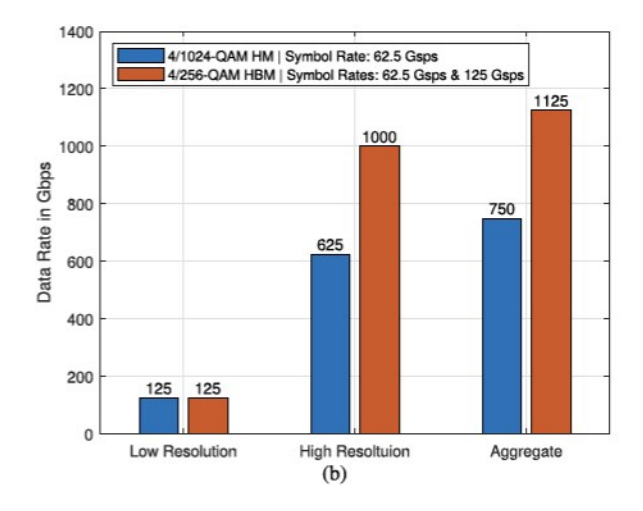


Fig. 12. The Functional Region for the 4/16 QAM HBM System.

for the high resolution receiver, when λ is equal to zero, it is impossible to differentiate the high resolution symbols, which results in the highest error rate for this receiver. The high resolution receiver instead does best when λ is equal to 1, which corresponds to a uniform 16-QAM constellation. We would expect the high resolution receiver to prefer this scenario because all the symbols are equi-distant from each other, which minimizes the possibility that symbols are mistaken for each other. In order to find a value of λ for which both receivers are functional we define a threshold SER that both receivers must operate below. From this threshold it is easy to identify the range of λ values that allow both receivers to operate below the threshold. As is labeled in Fig. 12, for an SER threshold of 10^{-3} the functional region for the system described above with receivers at 3m and 12m exists between about 0.25 and 0.75. Although most wireless communication systems require an SER $< 10^{-6}$, this threshold was picked so that the error rate could be experimentally represented within one frame.

To consider the generalized expressions for SER, the functional region was also explored for a 4/64-QAM HBM system with receivers at 3m and 6m. For M = 64, the expected error rates can be found using (18) and (17).



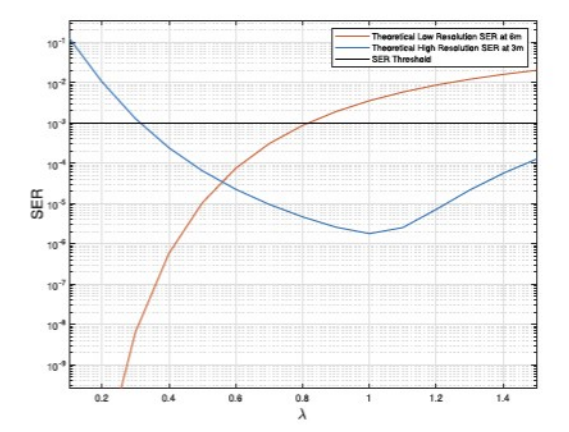


Fig. 13. Functional Region for the 4/64-QAM HBM System.

The functional region can be found for a 4/M-QAM system as described above for the 4/16-QAM. For a given SER threshold of 10^{-3} , the functional region of a 4/64-QAM is shown in Fig. 13 to exist between about 0.3 and 0.8.

In LoS scenarios, the HBM functional region depends heavily on the receiver distances, and Fig. 14 shows the SER as a function of λ for various distances. The performance of receivers demodulating the low resolution information and the high resolution information is shown by the dashed and solid lines respectively. In both instances, an increased transmission distance results in a worse performance at all values of λ . Thus λ s providing an SER below the desired threshold decreases. In other words, as receivers move farther away from the transmitter, the functional region shrinks to a smaller range of λ values.

B. HBM Systems With Mobile Receivers

The functional region offers an important design consideration for implementing an HBM system when the transmission distances or range of transmission distances are known. After determining the proper value of λ for the transmitter, receivers still must determine which resolution they should demodulate. One advantage HBM systems have over non-hierarchical

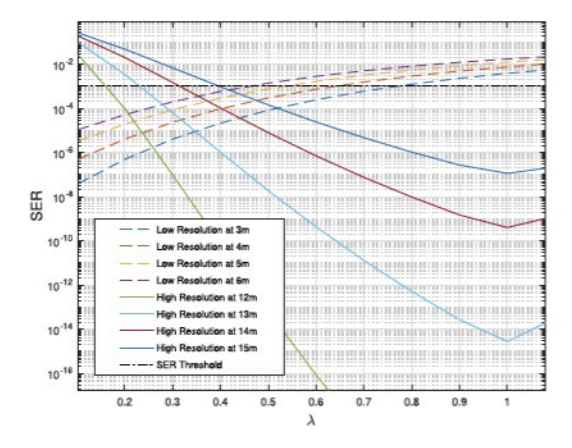


Fig. 14. Functional Region for the 4/16-QAM HBM System for various distances.

systems is their flexibility in this case. When a receiver's bandwidth or SNR changes, the receiver can adjust accordingly to receive the maximum amount of information with an acceptable error rate. Any number of changes in the surrounding environment can cause such fluctuations, and the receiver will need to determine which resolution is best to achieve acceptable SER values. Assuming a system that performs equalization, the equalization process must be done on a per-frame basis and for the receiver's chosen resolution. For this reason, receivers should avoid switching resolutions within a frame.

Although more research needs to be done for receivers to be able to estimate their available bandwidth, a simple SNR or $\frac{E_s}{N_0}$ estimate would provide a strong indication of which resolution can be successfully demodulated in a given channel. Since these estimates must be performed for each frame, the strength of the header can be used to determine the $\frac{E_s}{N_0}$. From there, the $\frac{E_s}{N_0}$ estimate should be compared to thresholds determined by the target SER. The $\frac{E_s}{N_0}$ threshold can be found using equation 17. The goal is to find the range of $\frac{E_s}{N_0}$ such that

$$SER_{HighResTh} > SER_{HighRes} \left(\frac{E_s}{N_0}, \lambda \right).$$
 (24)

The lower bound of this region can be called $\frac{E_s}{N_0 T_h H i q h}$ and will correspond to the maximum distance the high resolution information can be successfully transmitted. λ would be kept constant in these expressions since it is a physical layer parameter that would have already be established. Theoretically, if the estimated $\frac{E_s}{N_0}$ is above $\frac{E_s}{N_0}$, the receiver should use the high resolution, while if it is below the threshold, the receiver should use the low resolution. However, there could be a few areas of concern when a receiver nears this threshold. First, given that the $\frac{E_s}{N_0}$ estimate is taken at the beginning of the frame, there is a possibility that the $\frac{E_s}{N_0}$ is just above the threshold when the estimate is taken, but falls below the threshold as the rest of the frame is received. This would likely result in an SER above the determined maximum. To combat this issue, the $\frac{E_s}{N_0}$ threshold should be adjusted by a parameter α that depends on how quickly the channel is expected to change and on the frame duration.

Another possibly problematic situation could occur if a receiver's $\frac{E_s}{N_0}$ is fluctuating rapidly around $\frac{E_s}{N_0 ThHigh}$. In this case, the receiver might switch resolutions very frequently, or after switching to the high resolution the $\frac{E_s}{N_0}$ might fall back below $\frac{E_s}{N_0 ThHigh}$ in the middle of a frame resulting in a high SER. These problems can be addressed by establishing a *transition region* in which a receiver could use either resolution. Thus while a receiver will switch from the high resolution to the low resolution at

$$\frac{E_s}{N_0}_{HighLowTh}[dB] = \frac{E_s}{N_0}_{ThHigh}[dB] + \alpha[dB], \quad (25)$$

receivers should switch from the low to the high resolution at

$$\frac{E_s}{N_0} \sum_{LowHighTh} [dB] = \frac{E_s}{N_0} \sum_{ThHigh} [dB] + \alpha [dB] + \beta [dB],$$
(26)

where β is a function of how quickly the channel fluctuates, the frame duration, and the number of subsequent frames that should be demodulated with the same resolution.

VII. RESULTS

A. Simulated Results

In this section we verify the expressions obtained in Sec. IV through a full end-to-end MATLAB simulation of an HBM system.

The results are compared with our expressions to obtain the plot shown in Fig. 15a and Fig. 15b. The simulated system involves encoding of a bitstream into a grey coded HBM constellation, modulating the constellation symbols onto a 130 GHz digital signal, adding Additive White Gaussian Noise (AWGN), and implementing separate correlating demodulators for the high resolution and low resolution receivers. Because 130 GHz exists inside an absorption-free window, the absorption loss is negligible. For this simulation, a constant value of $\lambda=0.6$ is used, and the SER is calculated by sweeping the $\frac{E_s}{N_0}$ values. As can be seen in both Fig. 15a and Fig. 15b, the high resolution simulated and theoretical values align nearly perfectly.

Now that we have verified our error rate expressions through simulations, we proceed to use experiments to verify the functional region's existence.

B. Experimental Set-up

Our experimental system, described in [28] and [29] and shown in Fig. 16, operates at 130 GHz where absorption losses are negligible. Thus, we do not see the distance-dependent bandwidth in our experiments, but we use the test bed to validate the concepts presented. The transmitted signal is generated in baseband using MATLAB before it is uploaded to the Arbitrary Waveform Generator (AWG) labeled on the right side of Fig. 16. The AWG converts the discrete MATLAB signal into an analog signal that is then mixed with a 130 GHz sinusoidal signal on the system front-end shown in Fig. 17. The 130 GHz signal is generated from a local oscillator signal that has passed through two frequency doublers. After mixing,

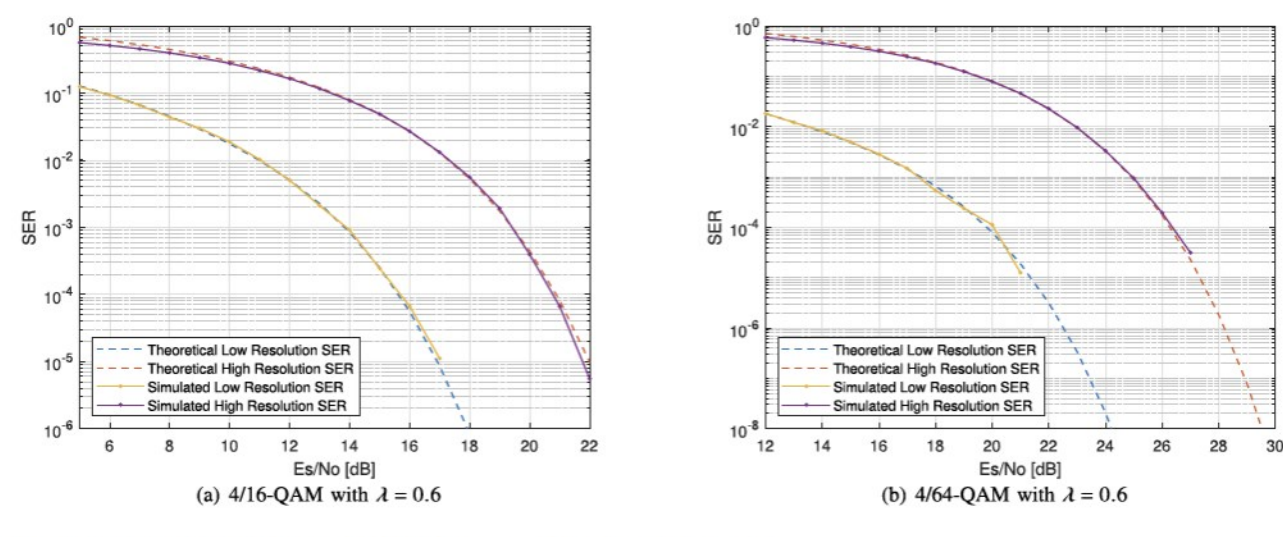


Fig. 15. Comparison of the SER for simulated HBM systems and the theoretical equations.

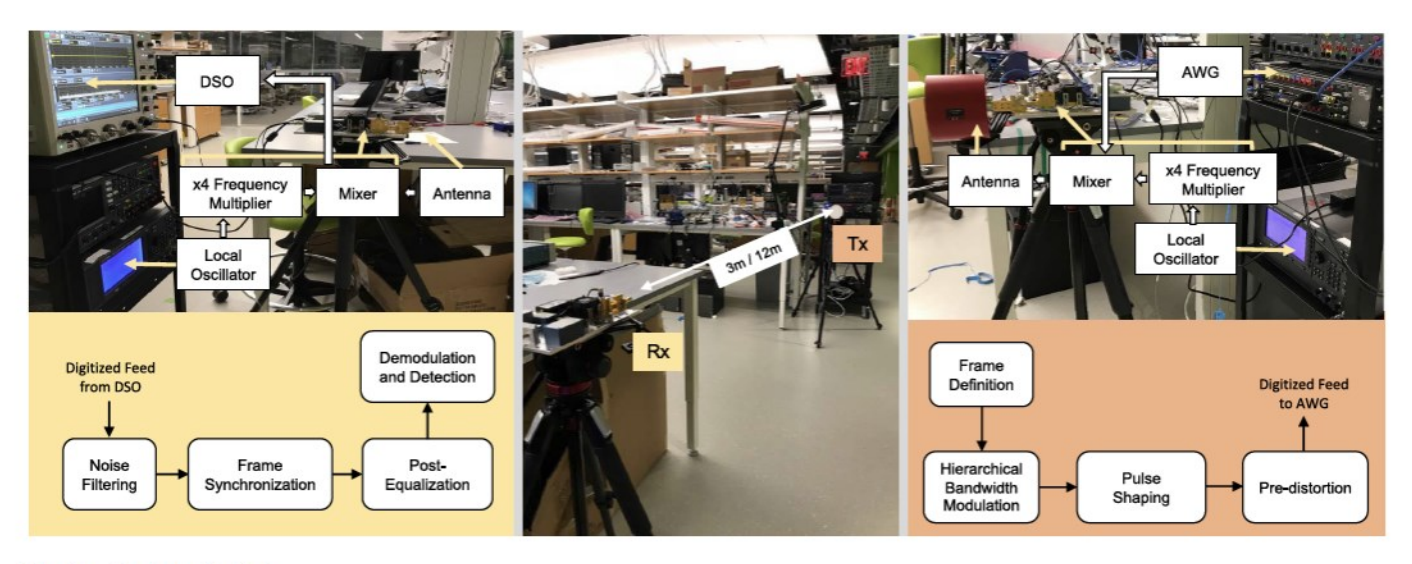


Fig. 16. TeraNova Testbed.

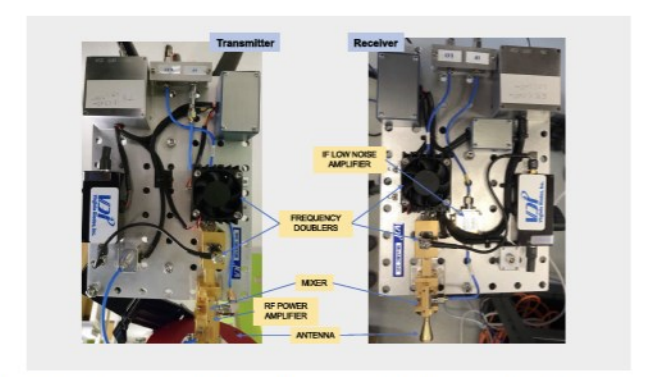


Fig. 17. Transmitter (left) and receiver (right) front-ends used for experiments.

the modulated signal is amplified using a RF power amplifier before it is radiated with a transmit power of 13 dBm using a directional antenna with a gain of 38 dBi.

On the receiver end, a 21dBi antenna is used, which is immediately followed by a mixer. The mixer demodulates the

signal using its own local oscillator signal that has also passed through two frequency doublers. The demodulated signal is amplified using a low noise amplifier at the intermediate frequency (IF) before it is captured in baseband by the Digital Storage Oscilloscope (DSO). Frame synchronization, noise filtering, equalization, and detection are all performed in MATLAB. Since only one receiver was available, the system was first set up with the transmitter and the receiver three meters apart. All the signals were sent and captured before the receiver was moved to the farther distances and the process repeated.

The frame structure of the data starts with an 18-bit maximal merit factor (MF) header for time synchronization at the receiver. 240 pilot bits are modulated as base-layer signals used for equalization by both receivers, with an additional 480 high resolution pilot bits modulated on top for the high resolution receiver's equalization. The data portion of the frame consists of 12000 base-layer bits and 24000 high resolution bits modulated onto a non-uniform QAM as was shown in Fig. 2. For this experiment a low resolution bandwidth of

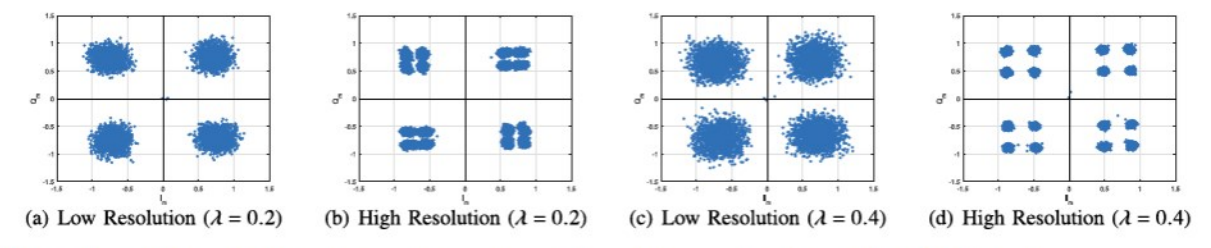


Fig. 18. Received constellations for high and low resolution receivers at 3m and 12m respectively for a 4/16-QAM HBM system.

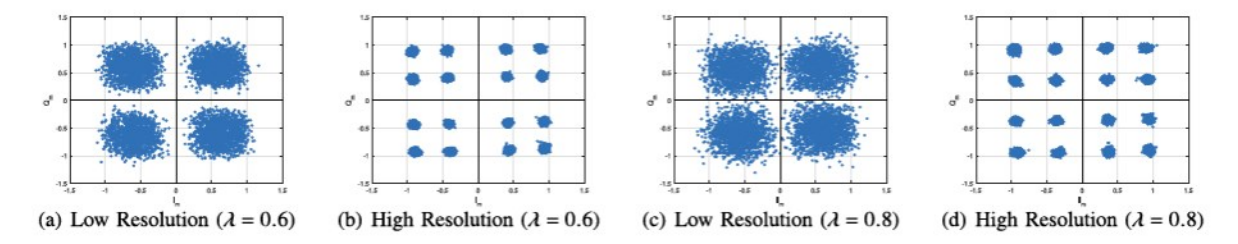


Fig. 19. Received constellations for high and low resolution receivers at 3m and 12m respectively for a 4/16-QAM HBM system.

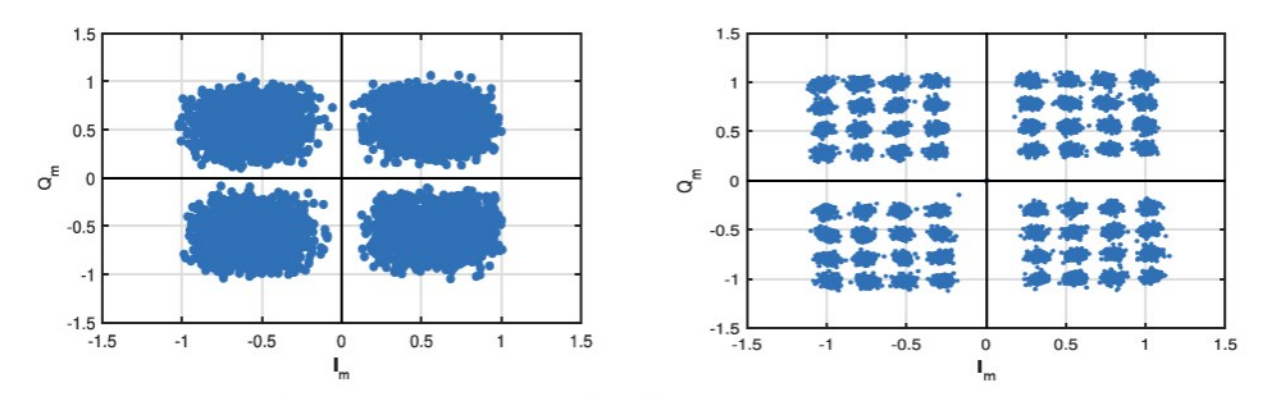


Fig. 20. Received Constellation by the far and near receivers in the 4/64-QAM system with $\lambda = 0.4$.

5 GHz and a high resolution bandwidth of 10 GHz are used for symbol rates of 2.5 Gsps and 5 Gsps at the low and high resolution receivers respectively.

C. Experimental Results

The goal of these experiments is to verify the calculated functional region in Fig. 12 and to prove its existence. Reviewing the experimental results for the 4/16-QAM, summarized in Table I, we observe what we expected; for values of λ outside the functional region (i.e. 0.2 and 0.8), one receiver is unable to demodulate with an SER below the established threshold, and for values of λ within the functional region (i.e. 0.4 and 0.6), SER values are all below the desired threshold. The results also show that outside the functional region, the receivers we expected to be functional and non-functional are behaving as expected. For instance, when λ is equal to 0.2, the low resolution receiver is expected to do well while the high resolution receiver struggles. Table I verifies that this is the case, since for the signal with $\lambda = 0.2$, the low resolution SER is very low, while the high resolution SER is above the desired threshold at 0.0028 in Fig. 18.

In the same way, on the other side of the functional region, when λ is equal to 0.8, Fig. 19 shows that the high resolution

TABLE I
EXPERIMENTAL RESULTS FOR DEMONSTRATING THE HBM FUNCTIONAL
REGION FOR 4/16QAM SYSTEM

λ	Low Resolution SER	High Resolution SER
0.2	8.33 * 10 ⁻⁴	0.0028
0.4	< 4.17 * 10 ⁻⁴	1 * 10 ⁻⁴
0.6	< 8 * 10 ⁻⁵	< 4 * 10 ⁻⁵
0.8	0.005	2 * 10-4

receiver is still successfully demodulating its information, but the symbols have spread out enough that the low resolution receiver is struggling. Meanwhile for λ values within our functional region, both receivers are able to successfully demodulate their symbols. In Fig. 18 and Fig. 19 the constellations are all successfully demodulated with symbol error rates below the 10^{-3} threshold. These results correspond with our analysis of Fig. 12. The experimental results using a 4/64-QAM HBM system are summarized in Table II, and they also verify the expected functional region shown in Fig. 13. As expected, the near receiver cannot demodulate below the desired threshold of 10^{-3} when $\lambda=0.2$, while the far receiver can demodulate successfully. For λ values of 0.4 and 0.6, both receivers are able to demodulate successfully, but for $\lambda=0.9$, which

TABLE II
EXPERIMENTAL RESULTS FOR DEMONSTRATING THE HBM FUNCTIONAL
REGION FOR 4/64-QAM SYSTEM

λ	Low Resolution SER	High Resolution SER
0.2	1.25 * 10 ⁻⁴	0.0112
0.4	< 8.3 * 10 ⁻⁵	2.167 * 10 ⁻⁴
0.6	6.667 * 10 ⁻⁴	8.33 * 10 ⁻⁵
0.9	0.0038	1 * 10-4

is outside the functional region, the low resolution receiver cannot demodulate at an SER below the desired threshold. An example of the received constellation for this experiment is shown in Fig. 20.

VIII. CONCLUSION

The design approaches and results presented in this paper prove that HBM successfully takes advantage of the bandwidth available for each receiver. The performance of HBM was characterized mathematically and proven with simulations and experiments. The HBM functional region was defined and proven to provide a range of λ values for which an HBM system is functional, and the transition region was suggested for HBM systems with fluctuating channels.

Continuing this work would involve generalizing the design expressions for more constellations and more than two resolutions. Additionally, the effect λ has on the $\frac{E_g}{N_0}$ ratio could be characterized further. Peak-to-average-power ratio (PAPR) is a drawback to high order QAM systems. A properly designed HBM signal would never perform worse than a uniform QAM in terms of PAPR, because recalling our analysis in Sec. VI-A, receivers will always prefer λ values less than 1. Still, a deeper study of how the PAPR can be considered in designing and analyzing the performance of HBM systems would be important. More work could also be done to evaluate coding and error correction schemes. Some coding and error correction strategies have been proposed for THz in [30], but there is still more to consider for the specific modulation schemes being presented in THz, including HBM in this field.

HBM also has potential in network applications. For networks using directional antennas, users are often multiplexed into different sectors while users within the same sector would receive the same information [31]. With HBM, however, it would be possible to multiplex users that are along the same transmission line but at different distances as well. For this use-case HBM would be implemented along side a multiple access protocol, in which receivers communicate with the transmitter using a regular non-hierarchical waveform in the up-link. The security of HBM systems has also been an important question, and as THz systems continue to be designed and implemented, security measures could be taken at these higher layers of the protocol stack. HBM would also be more versatile if both transmitters and receivers had a way to quickly determine how they were positioned with respect to each other, so improved channel estimation techniques in the THz band would be helpful for designing HBM systems as well. Given the many exciting opportunities and possibilities for HBM in the future of wireless communications and

THz communications specifically, more work should be done exploring these considerations.

APPENDIX A SER FOR 4/M-QAM HBM SYSTEMS

In the high resolution scenario, the non-uniform PAM that corresponds to a 4/M-QAM yields an error rate of

$$SER_{PAM} = \frac{2}{\sqrt{M}} \left((\sqrt{M} - 2)Q \left(\frac{d_2}{\sqrt{\frac{N_0}{2}}} \right) + Q \left(\frac{d_1}{\sqrt{\frac{N_0}{2}}} \right) \right), \tag{27}$$

where M is the high resolution constellation order and is assumed to be a power of 4. $\sqrt{M}-2$ gives the number of opportunities a constellation point could be received incorrectly if the noise pushed it a distance of d_2 . Also note that in the non-uniform PAM only one constellation point on either side of the origin can travel a distance of d_1 before it is incorrectly demodulated. To extrapolate for a 4/M-QAM we use the same method and approximation as we did for the 4/16-QAM to show that

 $SER_{HighRes}$

$$= \frac{4}{\sqrt{M}} \left(\left(\sqrt{M} - 2 \right) Q \left(\frac{d_2}{\sqrt{\frac{N_0}{2}}} \right) + Q \left(\frac{d_1}{\sqrt{\frac{N_0}{2}}} \right) \right). \tag{28}$$

In the low resolution case, the non-uniform PAM error rate can be shown as

 SER_{PAM}

$$= \frac{4}{M} \left[Q \left(\frac{d_1}{\sqrt{\frac{N_0}{2}}} \right) + Q \left(\frac{2 \left(\frac{\sqrt{M}}{2} - 1 \right) d_2 + d_1}{\sqrt{\frac{N_0}{2}}} \right) \right. \\
+ \frac{\sqrt{M}}{2} Q \left(\frac{\left(\frac{\sqrt{M}}{2} - 1 \right) d_2 + d_1}{\sqrt{\frac{N_0}{2}}} \right) \\
+ \sum_{n} \left\{ ((2n - 1) + 1) \left(Q \left(\frac{(2n - 1)d_2 + d_1}{\sqrt{\frac{N_0}{2}}} \right) \right. \\
+ Q \left(\frac{\left((2n - 1) + 1 \right) d_2 + d_1}{\sqrt{\frac{N_0}{2}}} \right) \\
+ Q \left(\frac{\left(\frac{\sqrt{M}}{2} - 1 + (2n - 1) \right) d_2 + d_1}{\sqrt{\frac{N_0}{2}}} \right) \\
+ Q \left(\frac{\left(\frac{\sqrt{M}}{2} - 1 + (2n - 1) + 1 \right) d_2 + d_1}{\sqrt{\frac{N_0}{2}}} \right) \right] \right].$$
(29)

Using (7), this expression can be approximated to

 SER_{LowRes}

$$=\frac{8}{M}\bigg[Q\left(\frac{d_1}{\sqrt{\frac{N_0}{2}}}\right)+Q\left(\frac{2\left(\frac{\sqrt{M}}{2}-1\right)d_2+d_1}{\sqrt{\frac{N_0}{2}}}\right)$$

$$+\frac{\sqrt{M}}{2}Q\left(\frac{\left(\frac{\sqrt{M}}{2}-1\right)d_{2}+d_{1}}{\sqrt{\frac{N_{0}}{2}}}\right)$$

$$+\sum_{n=1}^{\left(\frac{\sqrt{M}}{4}+1\right)\frac{1}{2}}\left\{\left((2n-1)+1\right)\left(Q\left(\frac{(2n-1)d_{2}+d_{1}}{\sqrt{\frac{N_{0}}{2}}}\right)\right)$$

$$+Q\left(\frac{\left((2n-1)+1\right)d_{2}+d_{1}}{\sqrt{\frac{N_{0}}{2}}}\right)$$

$$+Q\left(\frac{\left(\frac{\sqrt{M}}{2}-1+(2n-1)\right)d_{2}+d_{1}}{\sqrt{\frac{N_{0}}{2}}}\right)$$

$$+Q\left(\frac{\left(\frac{\sqrt{M}}{2}-1+(2n-1)+1\right)d_{2}+d_{1}}{\sqrt{\frac{N_{0}}{2}}}\right)$$

$$+Q\left(\frac{\left(\frac{\sqrt{M}}{2}-1+(2n-1)+1\right)d_{2}+d_{1}}{\sqrt{\frac{N_{0}}{2}}}\right)\right)\right\}\right].$$
(30)

Determining that E_s in this situation will be given by

$$E_{s} = \frac{1}{M} \left(4 \sum_{i=0}^{\frac{\sqrt{M}}{2} - 1} \sum_{j=0}^{\frac{\sqrt{M}}{2} - 1} \left((d_{1} + 2id_{2})^{2} + (d_{1} + 2jd_{2})^{2} \right) \right), \tag{31}$$

and rearranging to find an expression for d_1 yields

$$d_1 = \sqrt{\frac{ME_s}{8\sum_{i=0}^{\frac{\sqrt{M}}{2}-1}\sum_{j=0}^{\frac{\sqrt{M}}{2}-1}(1+2i\lambda+2j\lambda+2i^2\lambda^2+2j^2\lambda^2)}}.$$
(32)

We can use this expression to show the expected error rates as a function of $\frac{E_s}{N_0}$ and obtain the results given in (17) and (18).

ACKNOWLEDGMENT

The authors would like to thank to Jacob Hall for his help in collecting the data presented in this analysis and to Claire Parisi for her feedback on this paper.

REFERENCES

- T. S. Rappaport et al., "Wireless communications and applications above 100 GHz: Opportunities and challenges for 6G and beyond," *IEEE Access*, vol. 7, pp. 78729–78757, 2019.
- [2] Z. Hossain, Q. C. Li, D. Ying, G. Wu, and C. Xiong, "THz channel model for 6G communications," in *Proc. IEEE 32nd Annu. Int. Symp. Pers., Indoor Mobile Radio Commun. (PIMRC)*, Sep. 2021, pp. 1–7.
- [3] Cisco. (2020). Cisco Annual Internet Report (2018–2023).
 [Online]. https://www.cisco.com/c/en/us/solutions/collateral/executive-perspectives/annual-internet-report/white-paper-c11-741490.pdf
- [4] K.-C. Huang and Z. Wang, "Terahertz terabit wireless communication," IEEE Microw. Mag., vol. 12, no. 4, pp. 108–116, Jun. 2011.
- [5] I. F. Akyildiz, A. Kak, and S. Nie, "6G and beyond: The future of wireless communications systems," *IEEE Access*, vol. 8, pp. 133995–134030, 2020.
- [6] (Jun. 2021). Samsung Electronics and University of California Santa Barbara Demonstrate 6G Terahertz Wireless Communication Prototype. [Online]. Available: https://news.samsung.com/global/samsung-electronics-and-university-of-california-santa-barbara-demonstrate-6g-terahertz-wireless-communication-prototype
- [7] Z. Hossain and J. M. Jornet, "Hierarchical bandwidth modulation for ultra-broadband terahertz communications," in *Proc. IEEE Int. Conf. Commun. (ICC)*, May 2019, pp. 1–7.

- [8] J. M. Jornet and I. F. Akyildiz, "Channel modeling and capacity analysis for electromagnetic wireless nanonetworks in the terahertz band," *IEEE Trans. Wireless Commun.*, vol. 10, no. 10, pp. 3211–3221, Oct. 2011.
- [9] K. Sengupta, T. Nagatsuma, and D. M. Mittleman, "Terahertz integrated electronic and hybrid electronic-photonic systems," *Nature Electron.*, vol. 1, no. 12, pp. 622–635, Dec. 2018.
- vol. 1, no. 12, pp. 622–635, Dec. 2018.

 [10] B. Ning et al., "Prospective beamforming technologies for ultramassive MIMO in terahertz communications: A tutorial," 2021, arXiv:2107.03032.
- [11] D. Turchinovich, A. Kammoun, P. Knobloch, T. Dobbertin, and M. Koch, "Flexible all-plastic mirrors for the THz range," Appl. Phys. A, Mater. Sci. Process., vol. 74, no. 2, pp. 291–293, Feb. 2002.
- [12] X. Ma et al., "Intelligent reflecting surface enhanced indoor terahertz communication systems," Nano Commun. Netw., vol. 24, May 2020, Art. no. 100284.
- [13] W. Gao, Y. Chen, C. Han, and Z. Chen, "Distance-adaptive absorption peak modulation (DA-APM) for terahertz covert communications," *IEEE Trans. Wireless Commun.*, vol. 20, no. 3, pp. 2064–2077, Mar. 2021.
- Trans. Wireless Commun., vol. 20, no. 3, pp. 2064–2077, Mar. 2021.
 [14] C. Han and I. F. Akyildiz, "Distance-aware multi-carrier (DAMC) modulation in terahertz band communication," in Proc. IEEE Int. Conf. Commun. (ICC). Jun. 2014, pp. 5461–5467.
- Commun. (ICC), Jun. 2014, pp. 5461–5467.
 [15] C. Han, A. O. Bicen, and I. F. Akyildiz, "Multi-wideband waveform design for distance-adaptive wireless communications in the terahertz band," IEEE Trans. Signal Process., vol. 64, no. 4, pp. 910–922, Feb. 2016.
- [16] C. Lin and G. Y. Li, "Adaptive beamforming with resource allocation for distance-aware multi-user indoor terahertz communications," *IEEE Trans. Commun.*, vol. 63, no. 8, pp. 2985–2995, Aug. 2015.
- [17] A. Shafie, N. Yang, S. A. Alvi, C. Han, S. Durrani, and J. M. Jornet, "Spectrum allocation with adaptive sub-band bandwidth for terahertz communication systems," *IEEE Trans. Commun.*, vol. 70, no. 2, pp. 1407–1422, Feb. 2022.
- [18] A.-A.-A. Boulogeorgos, E. N. Papasotiriou, and A. Alexiou, "A distance and bandwidth dependent adaptive modulation scheme for THz communications," in *Proc. IEEE 19th Int. Workshop Signal Process. Adv. Wireless Commun. (SPAWC)*, Jun. 2018, pp. 1–5.
- Adv. Wireless Commun. (SPAWC), Jun. 2018, pp. 1–5.
 [19] P. Sen, H. Pandey, and J. M. Jornet, "Ultra-broadband chirp spread spectrum communication in the terahertz band," Proc. SPIE, vol. 11390, pp. 7–18, May 2020, doi: 10.1117/12.2558914.
- pp. /-10, May 2020, uoi. 10.1111/2.25367...
 K. Ramchandran, A. Ortega, K. M. Uz, and M. Vetterli, "Multiresolution broadcast for digital HDTV using joint source/channel coding," *IEEE J. Sel. Areas Commun.*, vol. 11, no. 1, pp. 6–23, Jan. 1993.
 K. Fazel and M. Ruf, "Combined multilevel coding and multiresolution
- [21] K. Fazel and M. Ruf, "Combined multilevel coding and multiresolution modulation," in *Proc. IEEE Int. Conf. Commun. (ICC)*, vol. 2, May 1993, pp. 1081–1085.
- [22] H. Jiang and P. A. Wilford, "A hierarchical modulation for upgrading digital broadcast systems," *IEEE Trans. Broadcast.*, vol. 51, no. 2, pp. 223–229, Jun. 2005.
- [23] S. Wang, S. Kwon, and B. K. Yi, "On enhancing hierarchical modulation," in *Proc. IEEE Int. Symp. Broadband Multimedia Syst. Broadcast.*, Mar. 2008, pp. 1–6.
 [24] A. Riaz, S. Ghafoor, and R. Ahmad, "Integration of millimeter-wave and
- [24] A. Riaz, S. Ghafoor, and R. Ahmad, "Integration of millimeter-wave and optical link for duplex transmission of hierarchically modulated signal over a single carrier and fiber for future 5G communication systems," *Telecommun. Syst.*, vol. 72, no. 2, pp. 221–229, Oct. 2019.
- Telecommun. Syst., vol. 72, no. 2, pp. 221–229, Oct. 2019.
 [25] S. Ju, Y. Xing, O. Kanhere, and T. S. Rappaport, "Millimeter wave and sub-terahertz spatial statistical channel model for an indoor office building," IEEE J. Sel. Areas Commun., vol. 39, no. 9, pp. 1561–1575, Jun. 2021.
- [26] S. Priebe and T. Kurner, "Stochastic modeling of THz indoor radio channels," *IEEE Trans. Wireless Commun.*, vol. 12, no. 9, pp. 4445–4455, Sep. 2013.
- [27] S. S. Haykin, Digital Communication Systems, vol. 1. Hoboken, NJ, USA: Wiley, 2014.
- [28] P. Sen, D. A. Pados, S. N. Batalama, E. Einarsson, J. P. Bird, and J. M. Jornet, "The TeraNova platform: An integrated testbed for ultrabroadband wireless communications at true terahertz frequencies," Comput. Netw., vol. 179, Oct. 2020, Art. no. 107370. [Online]. Available: https://www.sciencedirect.com/science/article/pii/S1389128620304473
- [29] P. Sen and J. M. Jornet, "Experimental demonstration of ultra-broadband wireless communications at true terahertz frequencies," in *Proc. IEEE* 20th Int. Workshop Signal Process. Adv. Wireless Commun. (SPAWC), Jul. 2019, pp. 1–5.
- [30] N. Akkari et al., "Joint physical and link layer error control analysis for nanonetworks in the terahertz band," Wireless Netw., vol. 22, no. 4, pp. 1221–1233, 2016.
- pp. 1221–1233, 2016.
 [31] K. P. Dasala, J. M. Jornet, and E. W. Knightly, "Uplink multi-user beamforming on single RF chain mmWave WLANs," in *Proc. IEEE Conf. Comput. Commun. (IEEE INFOCOM)*, May 2021, pp. 1–10.



Duschia Bodet (Student Member, IEEE) received the B.Sc. and M.Sc. degrees in electrical engineering from Northeastern University, Boston, MA, USA, in 2021, where she is currently pursuing the Ph.D. degree. With a concentration in wireless communications and signal processing, she interned at Raytheon in 2018 focusing on radar systems. In 2020, she also interned with the Air Force Research Laboratory, Griffiss Institute, to study modulation schemes for Terahertz communication systems.



Priyangshu Sen (Student Member, IEEE) received the B.Tech. degree from the Biju Patnaik University of Technology, India, in 2012, and the M.Tech. degree in radio-physics and electronics from the University of Calcutta, India, in 2015. He is currently pursuing the Ph.D. degree with the Department of Electrical and Computer Engineering, Northeastern University, Boston, MA, USA, under the guidance of Prof. Josep M. Jornet in UN Laboratory, MA, USA. In 2011, he completed his Industrial training at Garden Reach Shipbuilders and Engineers Ltd.,

on the communication system on naval board ship. In 2013, he started his career as a Research Engineer in radio-physics and electronics at the University of Calcutta. In 2019, he completed his summer training at Samsung Research America in the sub-Terahertz communication system and protocol design. His current research interests are in experimental and statistical characterization of Terahertz communication channel and networks.



Zahed Hossain (Member, IEEE) received the Ph.D. degree in electrical engineering from the University at Buffalo, The State University of New York (UB), in 2018. His work was completed at the University at Buffalo, as part of his Ph.D. work under the supervision of Prof. J. M. Jornet. He was a Lecturer with the University at Buffalo and taught signals and systems in the summer from 2014 to 2017. He is currently a Wireless Standards Systems Engineer with Intel Corporation. His current research interests include modulation, channel modeling, multi-user

interference modeling, protocol design, performance analysis and network simulation for Terahertz-band communication networks, with applications in terabit wireless personal and local area networks, beyond-5G/6G cellular networks, wireless nanosensor networks, and the Internet of Nano-Things. He was a recipient of the Best Paper Award for ACM NanoCom in 2017.



Ngwe Thawdar (Member, IEEE) received the B.Sc. degree in electrical engineering with minor in mathematics from the State University of New York Binghamton University in 2009 and the M.Sc. and Ph.D. degrees in electrical engineering from the State University of New York University, Buffalo, in 2011 and 2018, respectively. Since 2012, she has been with the Air Force Research Laboratory Information Directorate, Rome, NY, USA. Her research interests include wireless spread spectrum communications, cooperative communications and software-defined

radio implementation. Her latest research interest is on communications and networking in emerging spectral bands, such as mm-waves and terahertz band frequencies.



Josep M. Jornet (Senior Member, IEEE) received the B.S. degree in telecommunication engineering and the M.Sc. degree in information and communication technologies from the Universitat Politecnica de Catalunya, Barcelona, Spain, in 2008, and the Ph.D. degree in electrical and computer engineering from the Georgia Institute of Technology, Atlanta, GA, USA, in 2013. Between 2013 and 2019, he was a Faculty Member of the Department of Electrical and Computer Engineering, University at Buffalo, The State University of New York. He is currently

an Associate Professor with the Department of Electrical and Computer Engineering, the Director of the Ultrabroadband Nanonetworking Laboratory, and a Faculty Member of the Institute for the Wireless Internet of Things and the SMART Center, Northeastern University, Boston, MA, USA. He is serving as the lead PI on multiple grants from U.S. federal agencies including the National Science Foundation, the Air Force Office of Scientific Research, and the Air Force Research Laboratory as well as industry. His research expertise is in Terahertz communications, wireless nano-bio-communication networks, and the Internet of Nano-Things. In these areas, he has coauthored more than 200 peer-reviewed scientific publications, one book, and has also been granted six U.S. patents, which accumulate over 13,000 citations (H-index of 52) as of September 2022. He was a recipient of multiple awards, including the 2017 IEEE ComSoc Young Professional Best Innovation Award, the 2017 ACM NanoCom Outstanding Milestone Award, the UB Exceptional Scholar Young Investigator Award in 2018 and the Sustained Achievement Award in 2019, the NSF CAREER Award in 2019, the 2022 Martin W. Essigmann Excellence in Teaching Award, and the 2022 IEEE ComSoc RCC Early Achievement Award, among others. He has received multiple Best Paper Awards in multiple venues, including ACM NanoCom 2017, INFOCOM 2021, and the IEEE WoWMoM Non-Terrestrial Networks Workshop both in 2021 and 2022. He is an IEEE Distinguished Lecturer (Class of 2022-2023). He is also the Editor-in-Chief of the Nano Communication Networks journal (Elsevier) and the Editor of IEEE TRANSACTIONS ON COMMUNICATIONS.